ORIGINAL ARTICLE

A logical retrofit strategy optimization framework for resiliency bridge infrastructure management considering life-cycle cost

Pedram Omidian[a], Naser Khaji[b,*], Ali Akbar Aghakouchak[a]

[a] Faculty of Civil and Environmental Engineering, Tarbiat Modares University, P.O. Box 14115–397, Tehran, Iran.

[b] Civil and Environmental Engineering Program, Graduate School of Advanced Science and Engineering, Hiroshima University, 1-4-1, Kagamiyama, Higashi-Hiroshima, Hiroshima 739-8527, Japan.

*Corresponding Author: Naser Khaji. Email: nkhaji@hiroshima-u.ac.jp; Telefax: +81-82-424-7790.

Abstract: Bridges play an important role in providing essential services to communities as one of the most critical components of transportation infrastructure. In this regard, selecting reliable, robust, and efficient indicators is necessary to prepare a disaster management strategy. This study presents a multi-objective optimization framework for decision-makers to find the most optimal retrofit strategies that satisfy a given threshold of functionality/Resilience (R) while minimizing a structure's Life-Cycle Cost (LCC). Accordingly, various retrofit strategies include different materials (steel, Carbon Fiber Reinforced Polymer (CFRP), and Glass Fiber Reinforced Polymer (GFRP)), thicknesses, arrangements, and timing of retrofitting actions. In each scenario, the fragility curves are derived through nonlinear time-history Incremental Dynamic Analysis (IDA) to evaluate the LCC and resilience. In the subsequent step, the LCC analysis is conducted, considering the proposed formulation of multiple occurrences of seismic events, which incorporates the effects of complete/incomplete repair actions of damage conditions induced by previous seismic events. This study employs an elitist Non-dominated Sorting Genetic Algorithm II (NSGA-II) to identify the optimal set of solutions. The various aspects of the optimal retrofit strategies are thoroughly investigated and discussed for a bridge as a case study infrastructure. Results show that the considered objectives lead to reasonable and sense-making retrofit strategies.

Keywords: Resilience; life-cycle cost; infrastructures management; retrofit optimization framework; multiple occurrences hazards; damage accumulation

1 Introduction

One of the most critical functions of infrastructure systems, such as transportation networks, is to provide essential services to communities and to support their economic growth, security, and competitiveness. Bridges are one of the most common and crucial components in the transportation network, and they play vital roles in socio-economic activities such as providing logistics, emergency medical services, emergency routes for firefighting, and rescue operations in urban areas. However, bridges are constantly exposed to different natural hazard disasters, among which earthquakes are one of the most common and destructive natural phenomena that can cause various types of damage during their life-cycle [1]. Therefore, effective and dynamic decision-making frameworks must be used to correctly model interdependencies/dependencies, expected risks, and uncertainties that take into

account logical indicators. The total Life-Cycle Cost (LCC) is a rational economic index for under-study infrastructure during its life-cycle [2-3]. In this regard, the conventional seismic design approach is based on lower construction costs with an assumed level of performance as the set of criteria, which can eventually result in a non-economical option over the life-cycle of the infrastructure [4-5].

The Life-Cycle Cost Analysis (LCCA) is a powerful numerical tool in infrastructure management that assists decision-makers in choosing the optimal strategies [6-7]. Takahashi et al. [8] introduced an LCC optimization model using a renewal formulation of earthquake occurrences to minimize the expected LCC as a decision criterion. Frangopol and Liu [9] suggested a multiple-objective approach to balance the LCC and structure performance for managing and maintaining civil infrastructure with a focus on bridges. In this regard, research has been accomplished on developing the cost-effective in the form of the total life-cycle cost approaches to find the best strategy for manipulating infrastructure systems exposed to extreme natural disasters [10]. Zhu and Liu [11] presented a maintenance strategy optimization framework for Reinforced Concrete (RC) girder bridges by considering four separate objective functions, including condition index, reliability index, service life, and life cycle maintenance cost by performing Non-dominated Sorting Genetic Algorithm (NSGA). Omidian and Khaji [12] proposed a multi-objective optimization framework for seismic resilience improvement of RC structures by selecting the most optimal strategies optimized for the resilience index and the cost of retrofit using NSGA-II. In addition, a few research studies have been carried out to evaluate the ability to repair structures by estimating their structural functionality and the associated repair costs [13]. In these studies, different options were included in the LCCA to present the decision-makers, including repairing, upgrading or retrofitting, demolishing, and reconstructing under-study infrastructure.

In infrastructure management, proposing a sense-making methodology is becoming a high priority for policymakers as they seek to find optimal strategies for disaster risk reduction. In this connection, seismic resilience as another risk indicator is becoming a driving concept in the design, assessment, monitoring, maintenance, and management of infrastructure systems [14]. Resilience can be defined as the ability of a system to withstand the effects of disruptive events and efficiently recover to pre-event performance. In this respect, this research presents a sense-making optimization framework by examining and comparing various objectives, such as the life-cycle cost, cost of retrofit, and resilience index, through single- or multi-objective optimization. This framework presents a comprehensive understanding of the current- and future-state of the under-study system, which enables decision-makers to make informed decisions. This is achieved by developing a dynamic programming process to calculate the likelihood of different damage states occurring during each hazardous event. Also, as shown in a majority of the research on the LCCA, two probable repair scenarios that are considered for a specific damage state of a structure include (I) the action of repairing is accomplished before the next occurrence of a hazard event, where the structure returns to its intact state, or (II) it is assumed that the action of repairing is not completed before the following events, which may exacerbate the damage state by the following hazardous event. Therefore, this study employs a novel methodology for evaluating the probabilistic LCC of the under-study infrastructure exposed to multiple occurrences of a hazard type, which considers the consequences of complete/incomplete repair actions of damage states induced by previous seismic events. The introduced framework utilizes the total probability theorem and conditional probability chain rule to account for the uncertainties and dependencies between multiple hazardous occurrences. **Fig. 1** illustrates the flowchart of the optimization framework procedure of this study.

As shown in **Fig. 1**, the proposed multi-criteria optimization framework in this study comprises three main steps. In the first step, the characteristics of the under-study infrastructure and the site-specific hazard are determined (as explained in Section 4). For this purpose, a typical five-span RC box girder bridge is considered a case study infrastructure with different pier retrofit strategies, including ten different timeframes of retrofitting action, eight retrofitting arrangements, and three materials (i.e., Glass Fiber Reinforced Polymer (GFRP), Carbon Fiber Reinforced Polymer (CFRP), and steel) with four thicknesses. In addition, seismic risk with multiple occurrences is considered the main hazard at the under-study site. In the second step, the type of structural analysis should be selected to obtain structural responses and calculate the resilience index (as discussed in Section 2). For this purpose, a number of nonlinear time-history Incremental Dynamic Analysis (IDA) is performed to assess fragility
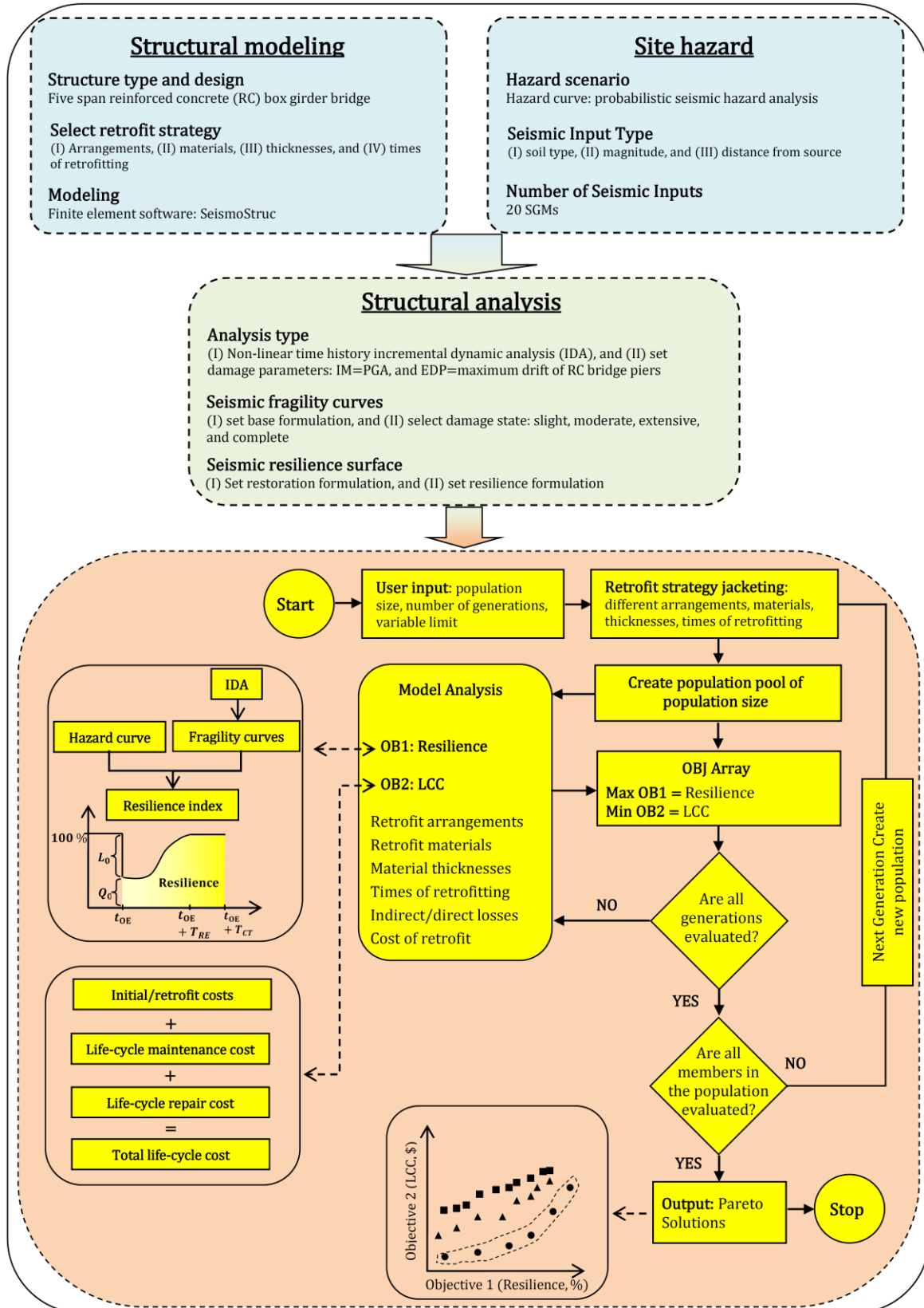
Fig. 1. A general overview of the optimization process of this study.

curves for each retrofit scenario, which are the foundation for constructing seismic resilience curves/surfaces. In the third step, the proposed multi-objective optimization framework is utilized to investigate different objectives (i.e., the LCC, the cost of retrofit, and the resilience index). In this step, the LCC is determined according to the hazard and fragility curves by assuming three involving costs:

(1) the cost of retrofit, (2) the life-cycle repair cost (including direct and indirect losses), and (3) the life-cycle maintenance cost during its service lifetime (as formulated in Section 3). In this respect, each strategy for retrofitting serves a unique purpose in reducing/increasing the total life-cycle cost and improving resilience index. Therefore, the widely recognized and efficient multi-objective optimization evolutionary algorithm NSGA-II was utilized in MATLAB platform [15] to identify the Pareto front or set of optimal solutions, in which the total life-cycle cost (or the cost of retrofit) is minimized while the resilience index is maximized (as presented in Section 5).

2 Theoretical foundations of resilience

In general, resilience $R(t)$ demonstrates the ability of infrastructure to sustain and recover to pre-event performance under hazard events, which can be determined by a predefined level of functionality $Q(t)$ within a control time (T_{CT}) [16]. Accordingly, some research in this field focuses on the numerical measurement of this concept in different infrastructure systems [17]. Mathematically, resilience index $R(t)$ is defined as a non-stationary stochastic process with a piecewise continuous function, which is the normalized highlighted area under the system functionality $Q(t)$ as follows:

$$R(t) = \int_{t_{0E}}^{t_{0E}+T_{CT}} \frac{Q(t)}{T_{CT}} dt \tag{1}$$

where t_{0E} indicates the time of occurrence of an event. To calculate the system functionality $Q(t)$, it is necessary to formulate two parameters of loss and recovery functions during the period of interruption as a consequence of the hazard event. From the mathematical viewpoint, this concept can be expressed as:

$$Q(t) = 100\% - [L(I, T_{RE}) \times \{H(t - t_{0E}) - H(t - (t_{0E} + T_{RE}))\} \times f_{rec}(t, t_{0E}, T_{RE})] \tag{2}$$

in which $L(I, T_{RE})$ demonstrates the loss function as a function of hazard intensity (I) and elapsed time to recover the infrastructure (T_{RE}). In addition, f_{rec} and $H(\cdot)$ indicate the post-event recovery path and the Heaviside step functions, respectively. Conceptually, the system functionality $Q(t)$ is equal to 100% for an ideal serviceable and intact system (or $R(t) = 100\%$). With a similar argument, this index falls $0 < Q(t) < 100\%$ when the system is damaged. In this regard, the loss of functionality directly after an extreme event (E) must be measured to evaluate the resilience index at this time (R_0). For this reason, the system functionality (Q_0) or resilience index (R_0) after any event (t_{0E}) can be calculated in terms of a dimensionless cost as $\left(\frac{\text{Cost of repair}}{\text{Replacement cost}}\right)$ based on the following relationship:

$$R_0(\%) = Q_0 = 100\% - \sum_k P_E(LS_k).r_k \tag{3}$$

where $P_E(LS_k)$ implies the kth structural limit state (e.g., slight, moderate, extensive, complete), which can be obtained from fragility curves. In addition, r_k is the damage ratio corresponding to the kth limit state derived following HAZUS [18].

2.1 Theoretical foundations of fragility and restoration curves

Because earthquake events have random natural characteristics, choosing a probabilistic approach to consider structures' seismic vulnerability is reasonable. In this regard, the Fragility curves describe the probability of reaching (or exceeding) a predefined level of structural damage state (i.e., slight, moderate, extensive, and complete as the kth damage state; DS_k) for a wide range of ground motion Intensity Measure (IM) levels. Selecting the appropriate Engineering Demand Parameter (EDP) and IM are critical to creating fragility curves. In this study, the Maximum Drift (MD) and Peak Ground Acceleration (PGA) are considered as EDP and IM for their efficiency, sufficiency, and practicality in seismic vulnerability assessment, respectively [19]. In a fully probabilistic seismic vulnerability assessment approach, the conditional probability $P_E(\cdot | \cdot)$ of demand being greater than the capacity can be calculated as:

$$P_E(D \geq DS_k | IM) = \phi \left[\frac{1}{\sigma_k} \ln \left(\frac{EDP}{\mu_k} \right) \right] \tag{4}$$

where $\phi[\cdot]$ is the log-normal Cumulative Distribution Function (CDF) with median value (μ_k) and log-standard deviation (σ_k) as the input fragility parameters for each damage state, which are chosen based on HAZUS [18] (see **Table 1**). In this study, the repair time of the case study bridge is considered following HAZUS [18] for four damage states. The restoration curve in HAZUS [18] for bridges typically shows the projected timeline for repairing or replacing a bridge after a disaster.

It is important to mention that the estimated repair times take into consideration delays in decision-making, financing, and inspection, and conducting inspections. They also serve as an approximation of the average time needed for highway bridges to fully recover their functions. Therefore, the amount of time required to repair a damaged bridge depends on the state of the damage. For each seismic damage state, the set of tasks that constitute the recovery path (or restoration function) along with the corresponding probabilistic models for required times are considered as (a) the time required for inspection and estimation, (b) the required time for preparing a repair plan, bidding, and contracting, (c) the time required for the mobilization of resources (i.e., materials and crews) and (d) the required time for repair. The HAZUS [18] methodology assumes the bridge capacity starts to recover right after the event and increases following a normal CDF. The HAZUS [18] normal CDF restoration model is expressed with median value (Mean) and standard deviation (SD) as presented in **Table 1**.

Table 1. Threshold of damage state quantities prescribed by HAZUS [18] for the initial intact state.

Damage State (DS_k)	Description of bridge pier	Fragility (drift)		Restoration (days)	
		μ_k	σ_k	Mean	SD
Slight	Minor spalling at the column	0.01	0.6	0.6	0.6
Moderate	Any column experiencing moderate cracking and spalling	0.025	0.6	2.5	2.7
Extensive	Any column degrading without collapse	0.05	0.6	75	42
Complete	Any column collapsing	0.075	0.6	230	110

3 Life-Cycle Cost Analysis (LCCA)

The total life-cycle cost, C_{TOT}, in an infrastructure throughout its service lifetime generally includes (I) initial construction costs C_{IN}, (II) total life-cycle maintenance costs C_M, and (III) total life-cycle repair costs resulting from hazard events like earthquakes C_{RP}. In this regard, it is important to calculate the expected value of these costs considering future uncertainties. The Net Present Value (NPV) is used to compare and calculate the discounted values of these costs in different years using the following relationship:

$$\bar{C}_{TOT,NPV} = \bar{C}_{IN} + \bar{C}_{M,NPV} + \bar{C}_{RP,NPV} \tag{5}$$

in which $\bar{C}_{TOT,NPV}$, $\bar{C}_{IN}$, $\bar{C}_{M,NPV}$, and $\bar{C}_{RP,NPV}$ represent the discounted NPV of C_{TOT}, C_{IN}, C_M, and C_{RP}, respectively. For an existing infrastructure, $\bar{C}_{IN}$ will be equal to zero in the LCC calculations. However, if there are plans to upgrade the infrastructure, $\bar{C}_{IN}$ equals the upgrade costs. In addition, routine maintenance intervention is frequently undertaken for infrastructure to uphold its performance in optimal conditions. In order to determine the annual NPV of the total life-cycle maintenance costs, the following relationship can be used

$$\bar{C}_{M,NPV} = \sum_{t=1}^{T_{LC}-1} \gamma^t \times C_M \tag{6}$$

in which C_M indicates the annual maintenance cost for the infrastructure and is assumed to remain constant each year during its service lifetime. Also, T_{LC} indicates the expected life-cycle of the under-study system. In addition, the annual discount factor, denoted by $\gamma = \frac{1}{1+r}$, is used to represent the discount rate. As shown in Eq. (6) for $\bar{C}_{M,NPV}$, the NPV of the expected life-cycle repair cost at different years can be calculated in a similar manner as follows:

$$\bar{C}_{RP,NPV} = \sum_{t=0}^{T_{LC}-1} \gamma^t \times \bar{C}_{RP,t} \tag{7}$$

where $\bar{C}_{RP,t}$ denotes the total expected repair cost incurred by the under-study infrastructure within the timespan of $[t, t+1]$. By using the law of the total probability, this term can be expressed as a correlation with the potential limit states that the infrastructure may face following the next hazard occurrences as:

$$\bar{C}_{RP,t} = \sum_{k=1}^{N_{LS}} \bar{C}_{rp}(LS_k) \times P_E(LS_k, [t, t+1]) \tag{8}$$

in which N_{LS} implies the total number of limit states, $\bar{C}_{rp}(LS_k)$ represents the expected repair cost at limit state k, and $P_E(LS_k, [t, t+1])$ indicates the likelihood of the system facing limit state k. Furthermore, $\bar{C}_{rp}(LS_k).P_E(LS_k, [t, t+1])$ can be referred to as the risk cost at limit state k and can be rewritten as the difference between the total risk cost of encountering limit state k within $[0, t+1]$ and $[0, t]$ as follows:

$$\bar{C}_{RP,t} = \sum_{k=1}^{N_{LS}} \{\bar{C}_{rp}(LS_k) \times P_E(LS_k, [0, t+1]) - \bar{C}_{rp}(LS_k) \times P_E(LS_k, [0, t])\} \tag{9}$$

Mathematically, it is probable that any unknown number (represented by n) of hazardous events (such as earthquakes) will happen during a specific timespan. Hence, by using the law of the total probability, the cumulative repair costs for the total number of events (n) during $[0, t]$ and each limit state k, may be calculated as:

$$\bar{C}_{rp}(LS_k).P_E(LS_k, [0, t]) = \sum_{n=1}^{\infty} P_{nt}(n, t) \left(\sum_{j=1}^{n} \{\bar{C}_{rp}(LS_k).P_E(LS_k^j \mid n, t)\} \right) \tag{10}$$

where $P_{nt}(n, t)$ represents the likelihood of n independent events occurring within a time interval $[0, t]$, calculated using a Poisson distribution with υ occurrence rate. The term $P_E(LS_k^j \mid n, t)$ denotes the probability of the system facing limit state k during the jth hazardous event. By utilizing $P_E(LS_k^j \mid n, t)$, the probability of unfinished (or incomplete) repair actions is considered to estimate the cumulative damage.

In order to determine the risk cost, one must first calculate $P_E(LS_k^j \mid n, t)$ as a measure of the likelihood of damage states exceeding a certain threshold for the under-study infrastructure. In Section 2, it is outlined that the fragility curves are determined by using the MD results from structural analysis, with specified median and log-standard deviation values for different levels of damage states. These levels correspond to slight, moderate, extensive, and complete damage states, which are considered as the 1st, 2nd, 3rd, and 4th seismic damage states based on **Table 1** and **Table 2** [2, 20]. Therefore, the likelihood of being at the limit state between damage state k and $k+1$ can be calculated as [18]:

$$P_E(LS_k) = P_E(DS_k) - P_E(DS_{k+1}) \tag{11}$$

The condition of post-event infrastructure following a hazardous event is typically determined by how the structure responds to different factors, including the intensity and type of hazard and incurred damage, by considering the damage situation of the infrastructure system prior to the next hazardous event. For example, if a hazard causes damage to a structure and repairs are underway to return the system to its intact state, another event occurring before the repairs are completed is likely to exacerbate the overall damage situation. In such scenarios, it is assumed that the damage situation is equivalent to the state of the system just prior to repairs starting. By applying the law of conditional probability, $P(DS_k^j \mid n, t)$ can be calculated by [2]:

$$P_E\big(DS_k^j \,\big|\, n,t\big) = \sum_{k'=1}^{N'_{LS}} \sum_{RS} P_E\big(DS_k^j \,\big|\, [RS_{k'}, LS^{j-1}{}_{k'}], IM, n, t\big) . P\big([RS_{k'} \,\big|\, LS^{j-1}{}_{k'}, IM, n, t]\big) \qquad (12)$$

$$. P_E\big([LS^{j-1}{}_{k'} \,\big|\, n, t]\big) . P(IM)$$

in which N'_{LS} is the total number of limit states that the structure may sustain right after the $(j-1)$th hazardous event, and k' implies the k'th structural limit state when the structure is not initially intact.

The likelihood of a specific hazard intensity, $P(IM)$, can be computed by using the hazard curves. Therefore, the term $P(IM)$ can be stated as $\frac{1}{v} . |\Delta\lambda(IM)|$, which $\Delta\lambda(IM)$ implies the exceedance rate of IM of the hazard. As previously stated, $RS_{k'}$ in Eq. (12) is the repair status, which shows whether the infrastructure has been recovered ($RS_{k'} = 1$) for each damage type or not ($RS_{k'} = 0$) after the $(j-1)$th hazardous event. Using Bayes' theorem, the likelihood of insufficient time for repairing the incurred damage from previous hazardous events can be written as:

$$P\big([RS_{k'} = 0 \,\big|\, LS^{j-1}{}_{k'}, n, t]\big) = \frac{P\big([RS_{k'} = 0, n, t \,\big|\, LS^{j-1}{}_{k'}]\big)}{P_{nt}(n,t)} \qquad (13)$$

Given that n hazardous events occur between $[0, t]$, the likelihood of an incomplete repair condition occurring at the jth hazardous event can be expressed as $P(t_j - t_{j-1} < \tau_{k'}, \{j - 2, [0, t_{j-1}]\}, \{0, [t_{j-1}, t_j]\}, \{n - j, [t_j, t]\})$, indicating that the time difference between the $(j-1)$th and (j)th hazardous events must be shorter than the time required for repair actions (i.e., $t_j - t_{j-1} < \tau_{k'}$). According to probability laws, it can be stated that n hazardous events can occur within the time interval of $[0, t]$, with $j - 2$ hazardous events happening before $[0, t_{j-1}]$ (denoted as $\{j - 2, [0, t_{j-1}]\}$). Also, the number of $n - j$ hazardous events should occur after jth hazardous event between $[t_j, t]$ (namely, $\{n - j, [t_j, t]\}$). In addition, it is necessary that no hazardous event take place between t_{j-1} and t_j (i.e., $\{0, [t_{j-1}, t_j]\}$) to satisfy the requirement of incomplete repair condition as follows:

$$P\big([RS_{k'} = 0, n, t \,\big|\, LS^{j-1}{}_{k'}]\big)$$
$$= \int_0^t \int_{t_{j-1}}^{\min\{t_{j-1}+\tau_{k'}, t\}} P(j - 2, [0, t_{j-1}]) . P(0, [t_{j-1}, t_j]) . P(n \qquad (14)$$
$$- j, [t_j, t]) . v^2 . dt_j . dt_{j-1}$$

As discussed in the total life-cycle cost analysis framework, fragility curves are one of the key components of presented computational framework. In this line, it was assumed that the structure's condition was intact or that the repair action was finished before the jth hazardous event.

Table 2. The ratio of median damage states for constrcuting fragility curves when a bridge is in intact condition compared to when it is not initially intact.

Damage state in fragility curve for initial intact limit state	Damage state in fragility curve for initial below limit state		
	Slight	Moderate	Extensive
Moderate	Moderate 1.25		
Extensive	Extensive 1.25	Extensive 1.5	
Complete	Complete 1.25	Complete 1.5	Complete 2

Therefore, it is necessary to establish new thresholds in order to construct fragility curves for damage states based on the condition in which a structure is damaged or repair actions are incomplete. Due to insufficient data, the ratio of median fragility curves when a bridge is in intact condition compared to when it is not, is obtained from **Table 2.** The ratios align with those reported by Raghunandan et al. [20] for RC structures, as there is a lack of reliable data for bridges. For example, considering Tables 1 and 2, the log-normal median drift of the fragility curve for the extensive limit state when the existing seismic damage state of the bridge is moderate is equal to 0.0167 ($= \frac{0.025}{1.5}$), compared to 0.025 when the structure is in its intact state. **Fig. 2** illustrates an overall flowchart of the

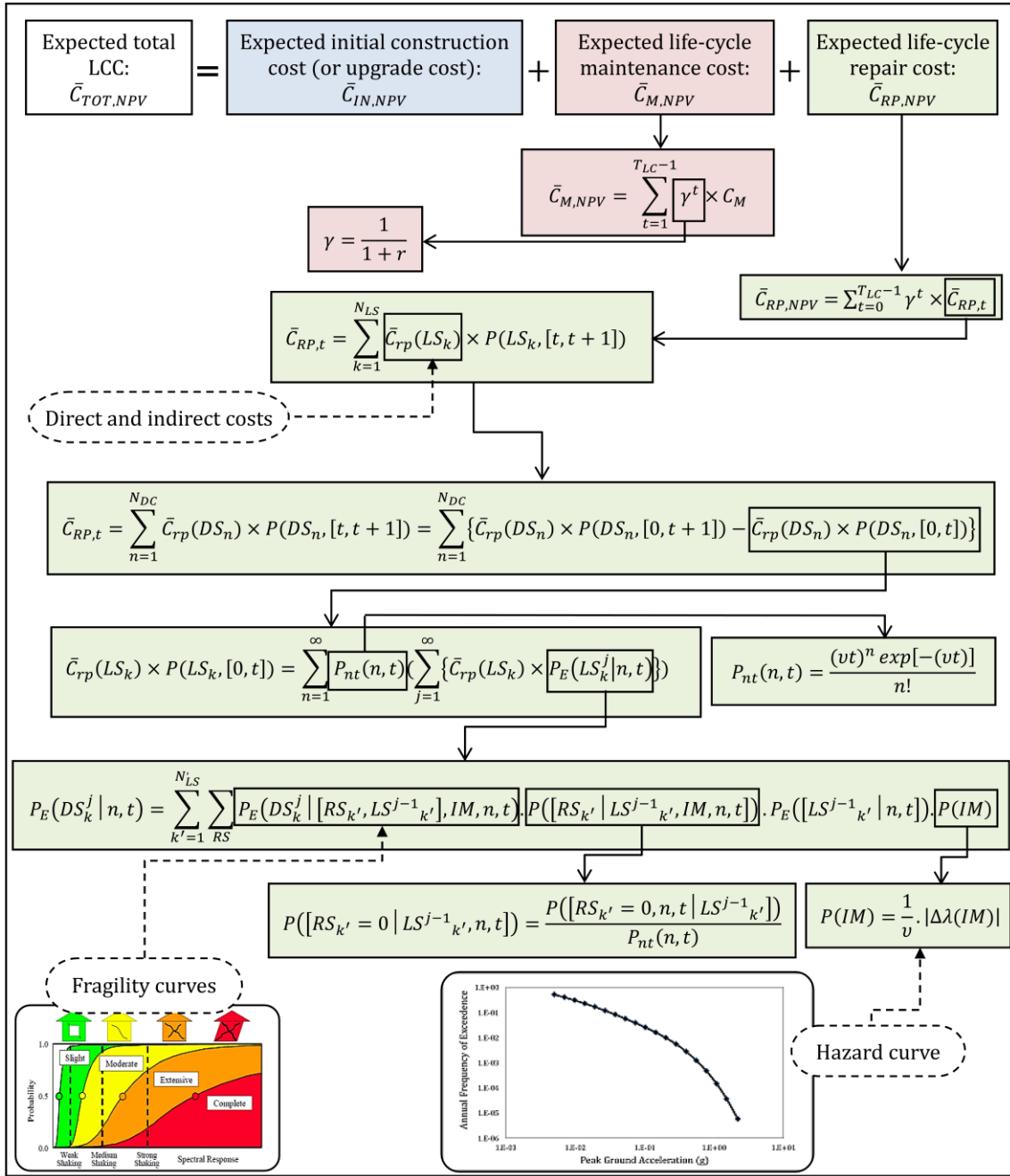LCC assessment framework for the infrastructure system.

Fig. 2. Flowchart for calculating the LCC assessment of infrastructure systems.

4 Modeling of illustrative case study

To implement the proposed Life-Cycle Cost and Resilience (LCC-R) optimization framework, the subject infrastructure should be selected in the first step, and potential natural hazards should be identified. In this regard, an RC box girder bridge, one of the most critical components in the transportation network, is considered a case study infrastructure, for which all steps of the optimization framework are discussed in detail. The considered RC box girder bridge is adapted from a bridge model presented by Sultan and Kawashima [21]. This bridge is assumed to be a three-lane with five spans (two 39.6 m exterior spans and three 53.3 m interior spans). **Fig. 3** demonstrates more details of the structure modeled in the finite element SeismoStruct platform [22], for which the beam and column sections' specifications are also presented.
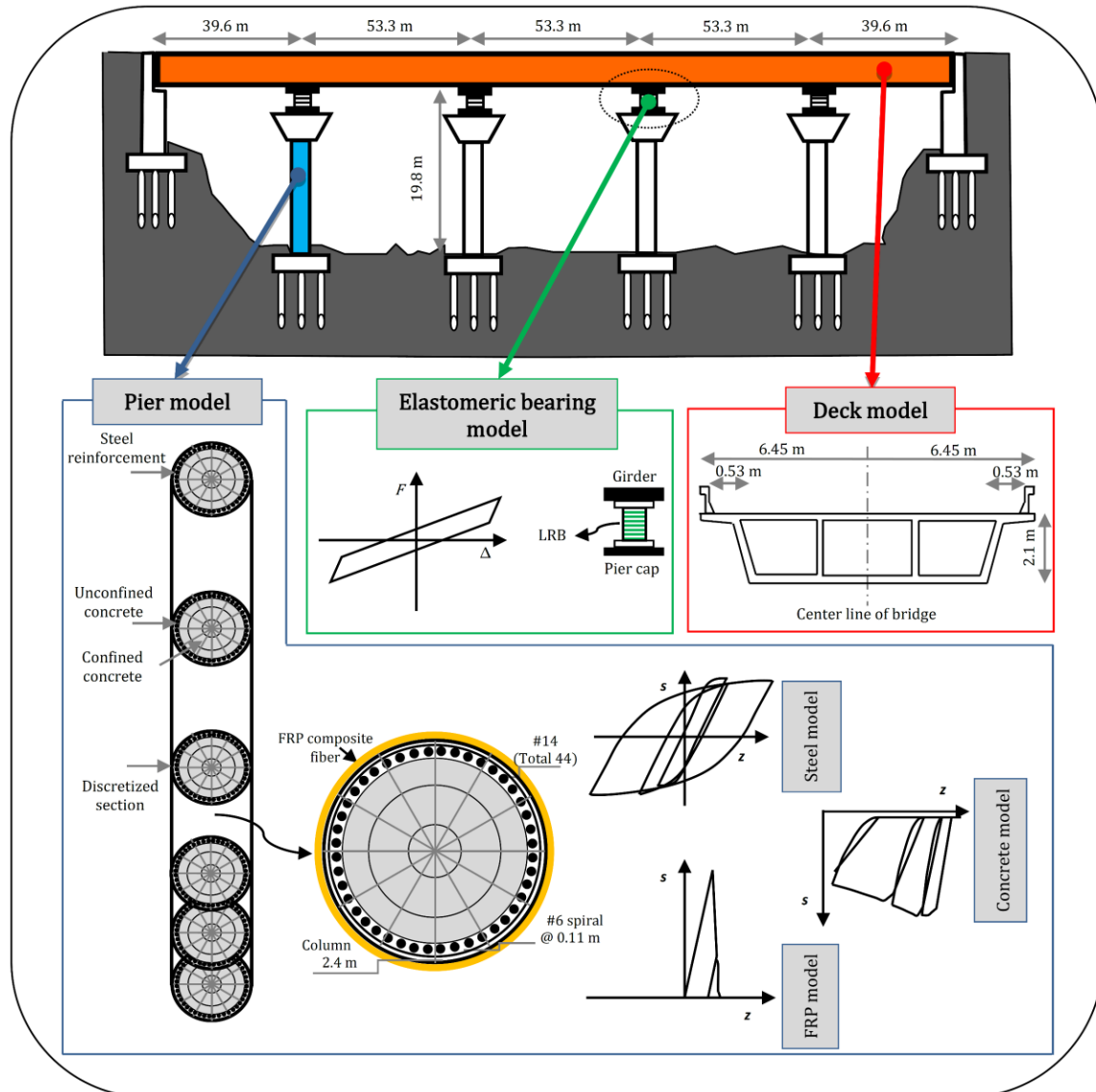
Fig. 3. Finite element model specifications of considered bridge in SeismoStruct software.

This research uses nonlinear time-history dynamic analysis to determine the structure's response. For material nonlinearity modeling, the 3D inelastic force-based frame element type is employed to define the structural elements in the SeismoStruct platform [22]. The concrete material is modeled using a uniaxial nonlinear variable confinement model, proposed by Madas and Elnashai [23], and the cyclic rules presented by Martinez-Rueda and Elnashai [24]. The reinforcement steel material is modeled using a uniaxial steel model initially programmed by Yassin [25], coupled with the isotropic hardening rules proposed by Filippou et al. [26]. The current implementation follows that carried out by Monti et al. [27]. Fragiadakis et al. [28] proposed an additional memory rule for higher numerical stability/accuracy under transient seismic loading. As for steel jacket material properties, a uniaxial bilinear stress-strain model with kinematic strain hardening is considered according to **Table 3**. For the Fiber Reinforced Polymer (FRP) confined concrete, Ferracuti and Savoia's model [29] is implemented, which follows the constitutive relationship and cyclic rules proposed by Yankelevsky and Reinhardt [30] under compression and tension states, respectively. Moreover, Ferracuti and Savoia's model employs Spoelstra and Monti's model [31] for the confining effect of jacketing materials. The FRP material is simulated using a simplified uniaxial trilinear FRP model that assumes no resistance in compression [32]. When the pier is jacketed by steel/FRP sheets, the cover concrete is considered as the concrete confined by the steel/FRP jacket, while the core concrete is regarded as the concrete confined by FRP and the transverse reinforcements.

Table 3. Material properties used in the finite element analysis.

Material	Mechanical property	Value
Concrete	Compressive strength (MPa)	35
	Tensile strength (MPa)	3.5
	Strain at peak stress (%)	0.2
Steel (bar)	Modulus of elasticity (GPa)	200.0
	Yield strength (MPa)	400
	Strain hardening parameters (%)	0.5
CFRP	Tensile strength (MPa)	930
	Tensile modulus (GPa)	89.6
	Ultimate elongation (%)	0.98
Steel (jacketing)	Modulus of elasticity (GPa)	200.0
	Ultimate tensile strength (MPa)	250
GFRP	Tensile strength (MPa)	587
	Tensile modulus (GPa)	27.4
	Ultimate elongation (%)	2.3

In order to retrofit the bridge piers, three different types of material (i.e., GFRP, CFRP, and steel) are utilized for pier jacketing purposes. Hence, steel jackets of four different thicknesses (T1 to T4) of 9.53, 12.7, 19.05, and 25.40 mm are selected. Furthermore, the piers are jacketed with 2, 4, 7, and 10 plies of CFRP and GFRP with 1.24 and 1.27 mm thicknesses for each ply, respectively. **Table 3** represents the specifications of the materials considered in this study. Additionally, eight different arrangements (A1 to A8) of the bridge's piers are considered for the retrofit plans, as shown by the red diagonal line pattern in **Fig. 4**, in which short names indicate the retrofitting arrangements. Moreover, different retrofitting plans are analyzed using three materials of different plies' thicknesses and numbers. In each case, the resilience index and the LCC are evaluated.
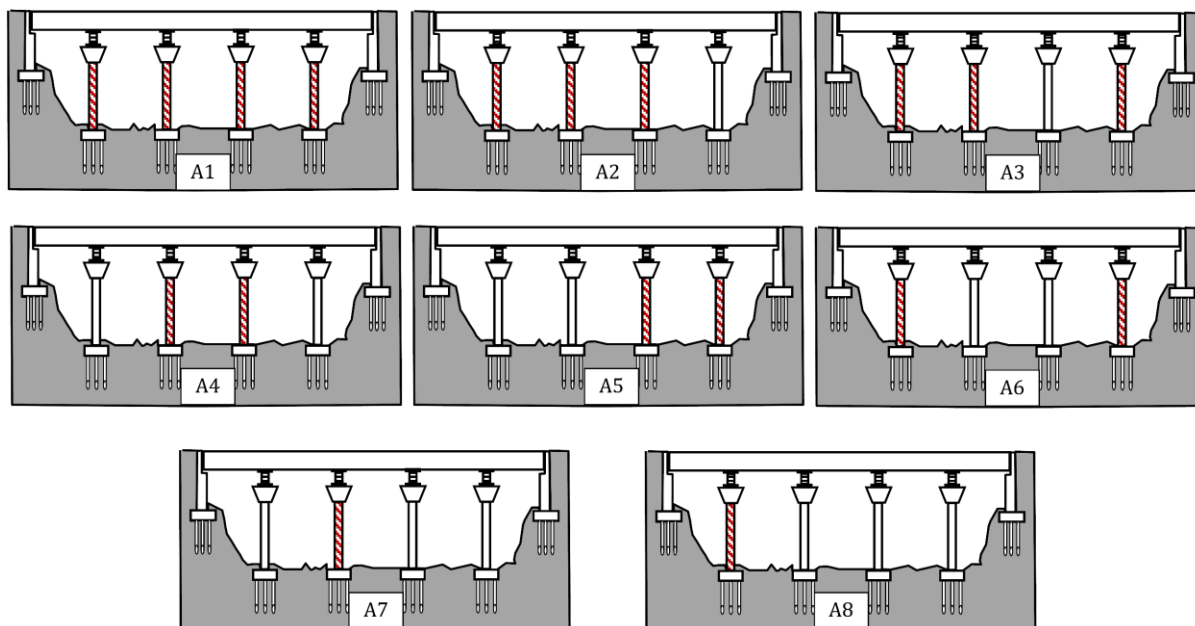
Fig. 4. Various arrangements used for bridge pier retrofitting configurations.

4.1 Strong ground motion selection and structural analysis

The fragility analysis, as an earthquake-induced structural damage index, is commonly carried out through the IDA method, which can be used to calculate the resilience surfaces and LCC. In this method, each Strong Ground Motion (SGM) record is scaled into a wide range of seismic intensity levels, and monotonically applied to the case study structure to extract different structural damage states from elastic to collapse. Therefore, selecting a reasonable number of suitable SGMs is necessary because the results are highly dependent on the characteristics of each record, and the procedure is time-consuming and costly. In this study, 20 time-histories are considered according to the recommendations

of Shome and Cornel [33] from the Pacific Seismic Engineering Research (PEER) database [34]. **Table 4** presents the SGM data, which correspond to an earthquake magnitude of approximately $5\sim7.5$, and the typical soil classification (i.e., $360 \leq V_{S30} \leq 760$ m/s). It should be noted that each record is scaled into ten stages from PGA = 0.1g to 1g by incremental step of PGA = 0.1g. In addition, an earthquake with a return period of 475 years is used to exclusively calculate the resilience index in the multi-objective optimization process, which results in PGA = 0.4g based on the Probabilistic Seismic Hazard Analysis (PSHA) of the under-study site (see **Fig. 2**).

Table 4. Strong ground motion records.

Record No.	Earthquake	Year	Station Name	Magnitude	R rupture (km)	PGA (g)	Focal Mechanism
1	Chichi	1999	CHY080	7.62	2.69	0.953	Reverse oblique
2	Northridge	1994	Sylmar - Converter	6.69	5.19	0.963	Reverse
3	Kobe	1995	Nishi-Akashi	6.9	7.08	0.498	Strike-slip
4	Erzincan	1992	Erzincan	6.69	4.38	0.488	Strike-slip
5	Loma Prieta	1989	Corralitos	6.93	3.85	0.662	Reverse oblique
6	Helena Montana	1935	Carroll College	6	2.86	0.196	Strike-slip
7	Nahanni Canada	1985	Site 1	6.76	9.6	1.019	Reverse
8	Corinth Greece	1981	Corinth	6.6	10.27	0.272	Normal oblique
9	Norcia Italy	1979	Cascia	5.9	4.64	0.213	Normal
10	Izmir Turkey	1977	Izmir	5.3	3.21	0.41	Normal
11	North. California	1941	Ferndale City Hall	6.4	44.52	0.115	Strike-slip
12	San Fernando	1971	Fairmont Dam	6.61	25.58	0.111	Reverse
13	Tabas Iran	1978	Boshrooyeh	7.35	24.07	0.106	Reverse
14	Imperial Valley	1979	Calipatria Fire Station	6.53	23.17	0.129	Strike-slip
15	Friuli Italy	1976	Codroipo	6.5	33.32	0.091	Reverse
16	Victoria Mexico	1980	SAHOP Casa Flores	6.33	39.1	0.1	Strike-slip
17	Irpinia Italy	1980	Bovino	6.9	44.62	0.046	Normal
18	Coalinga	1983	Cantua Creek School	6.36	23.78	0.288	Reverse
19	Kern County	1952	Taft Lincoln School	7.36	38.42	0.18	Reverse
20	Northern Calif	1954	Ferndale City Hall	6.5	26.72	0.203	Strike-slip

4.2 Cost terms

In the process of proposed multi-objective optimization, one objective is to minimize the total life-cycle cost. In this study, the costs of composite fabrics are provided by the manufacturer as $105.92/m^2 for CFRP and $31.65/m^2 for GFRP plies. Additionally, the cost of steel jacketing is $500/ton. In addition, the average replacement cost for RC bridges is about $1833/m^2 based on Caltrans [35]. As discussed in Section 3, the annual maintenance cost (C_M) in Eq. (6) is assumed to be constant and equals 0.5% of the bridge replacement cost for all years. In this line, the discount rate (r) has been estimated as 5% based on recommendations [36]. As previously highlighted, a set of direct and indirect losses are imposed on the community after each hazardous event due to the induced damage to infrastructure. As a result, a more rigorous assessment of these costs leads to a more reliable LCC. In this regard, the following set of costs are considered in this study: (1) costs of repairing, (2) costs of delay time, vehicle operation, and excess gas emission on users, (3) cost of economic losses, (4) cost of environmental damage, and (5) cost of human casualties. It should be noted that these costs are added together to evaluate the total cost for each limit state, i.e., $\bar{C}_{rp}(LS_k)$ in Eq. (8). The following is a brief discussion of each of the mentioned costs (for more detailed discussion, refer to [36]).

4.2.1 Agency repair costs

Based on HAZUS [18], agency-incurred repair costs can be calculated as r_k times the bridge replacement cost for each limit state. Also, as reported by Caltrans [37], two cost terms should be summed to the life-cycle repair cost, including (1) contingency and (2) mobilization costs, which are estimated as 20% and 10% of the bridge repair cost, respectively.

4.2.2 User costs of imposed delay, vehicle operation, and excess emission

To repair damaged components of the bridge, it is often essential that the bridge site be closed entirely or partially for the safety of workers and other users during this time. Therefore, user costs are incurred due to delays imposed on passengers, overwork of vehicles, and the release of excess hydrocarbons, carbon monoxide, and nitrous oxide due to such traffic disruptions [38]. This cost term,

$C_U(LS_k)$, can be calculated in the damage repair costs for the case study bridge according to the following relationship [37]:

$$PC_U(LS_k) = \min(\tau_k, 1/v) \times (t_{ij}^{D/R} - t_{ij}^O) \times [(AADT - AADTT) \times \rho_C + AADTT \times \rho_T] \qquad (15)$$

in which $\min(\tau_k, 1/v)$ denotes the expected time of traffic disruptions that is the minimum required repair time for the kth limit state (τ_k, according to **Table 1**) and the expected time difference between hazardous events. In addition, the Annual Average Daily Traffic ($AADT$) and the Annual Average Daily Truck Traffic ($AADTT$) of route ij take the values equal to 77000 and 7392, respectively. The t_{ij}^O and $t_{ij}^{D/R}$ are the time for passing route ij without and with partial/complete closure based on Bocchini and Frangopol [39], respectively. Finally, following the recommendations of the Ohio Department of Transportation [40], ρ_C and ρ_T are chosen at \$21.79/hour and \$58.83/hour, respectively.

4.2.3 Cost of economic losses

Businesses around the transportation network will be affected by traffic disruption due to bridge damage after a hazard occurrence and subsequent repair actions process. In this regard and considering such economic losses, twice the user cost of imposed delay, vehicle operation, and excess emission are considered based on Kliesen and Mill's research [41].

4.2.4 Cost of environmental damage

As discussed previously, repairing the bridge network causes traffic interruption and delay; thus, increasing air pollution, consumption of energy, and global warming is possible [42]. This cost can be estimated using the following:

$$C_E(LS_k) = C_{Env} \times \min(\tau_k, 1/v) \times \left[En_{Vij}^{D/R} - En_{Vij}^O\right] \qquad (16)$$

in which $En_{Vij}^{D/R}$ and En_{Vij}^O indicate the unit value of carbon dioxide emission at speeds of V_{ij}^O and $V_{ij}^{D/R}$ which are the average velocity of vehicles passing route ij before and after a hazard event based on Gallivan et al. [43], respectively. The unit cost of environmental damage term (C_{Env}) refers to Kendall et al. [44], which is considered \$33.49 per ton of carbon dioxide emission.

4.2.5 Cost of human casualties

One of the potential consequences of damage to the transportation network and bridges is human casualties, including injuries and deaths. This cost term, $C_H(LS_k)$, can be calculated as a function of the kth damage limit as follows:

$$C_H(LS_k) = \sum_{t=1}^{4} C_{SLt} \times CR_k^{SLt} \times NPAR \qquad (17)$$

in which C_{SLt} is the cost of human casualty for severity level threshold t, CR_k^{SLt} denotes the casualty rate for severity level threshold t and limit state k, and $NPAR$ indicates the total number of people at risk. These parameters for the case study bridge are adopted following Porter et al. [45], HAZUS [18], and Caltrans [46], respectively.

5 Optimal retrofit strategies

Optimization is an organized process to find the best possible solution (or set of solutions) for single-objective (or multi-objective) problems by considering the conditions and limitations, respectively. In such optimization problems, maximizing or minimizing the values of the objective functions is necessary. In this study, fragility curve is constructed based on the characteristics of the structure and site. Then, seismic resilience curves/surfaces and the LCC can be assessed according to the presented framework. For different retrofit strategies, the mentioned general steps are repeated. In

addition, different optimization objectives are examined in the form of Single-Objective (SOO) and Multi-Objective Optimizations (MOO) by utilizing NSGA-II. Hence, the optimization problems are categorized into three parts including (I) SOO, which minimizes the LCC as the only objective, (II) MOO-1, which minimizes the cost of retrofit and maximizes resilience index; and (III) MOO-2, which minimizes the LCC and maximizes seismic resilience. As stated, NSGA-II evolutionary algorithm has been cited in over 40,000 publications and has been widely applied in different structural engineering optimization problems, especially in RC structures [47]. The NSGA-II is a powerful tool for solving multi-objective optimization problems. It offers strengths such as effectively handling multiple objectives, elitism preservation, diversity maintenance, computational efficiency, and flexibility. However, it has weaknesses, including scalability issues, potential for stagnation, and difficulty handling discontinuous or non-smooth objective functions. In this line, Rahimi et al. [48] showed that the NSGA II could find a large number of Pareto solutions, strong performance of search algorithms as hyper-volume, acceptable spread indicator value, as well as the best average CPU time performance of all algorithms for all test scales among 19 under-study evolutionary multi-objective algorithms. This algorithm generates non-dominated fronts for a population size of N and M objective functions in one iteration. The time complexity of the algorithm employed by the NSGA-II is $O(MN^2)$. As the generation of non-dominated fronts consumes most of the computational time in the NSGA-II (excluding fitness evaluations), enhancing the speed of this algorithm can significantly improve the overall efficiency of the NSGA-II and other genetic algorithms that utilize non-dominated sorting. Also, Ghodousian et al. [49] discussed the use of fuzzy logic to predict the 28-day strength of different concretes based on linear regression and various fuzzy logic methods by nearest neighborhood clustering using a modified PSO algorithm. The basic concept of the optimization problem of the present study is formulated as presented in **Table 5**.

Table 5. Step-by-step procedure of the NSGA-II algorithm for LCC-R optimization problem.

Initialize	
	User input: population size (N_p), random initial population ($P_t \subset S$), number of generations t_{max}, variable limit
	Retrofit design: Arrangements (a: Various plans used for retrofitting configurations) **&** **Materials** (m: Steel, CFRP, GFRP) **&** **Jacket thickness**: (j: Steel jacketing: 9.53, 12.7, 19.05, 25.40mm CFRP jacketing: 2, 4, 7, 10 PLY (each ply=1.24mm) GFRP jacketing: 2, 4, 7, 10 PLY (each ply=1.27mm)) **&** **Time of retrofitting**: (ti: Various time of retrofitting used for LCC)
Start	
	While ($t < t_{max}$) do
	Generate offspring (Q_t)
	Mutate on Q_t
	Set $R_t = P_t \cup Q_t$
	Evaluate objective functions:
	Resilience index (a, m, j)
	Life-cycle cost (a, m, j, ti)
	(or **Cost of retrofit** (a, m, j))
	Apply non-dominated sorting on R_t:
	Maximize: **Resilience Index**
	Minimize: **Life-cycle cost** (or **Cost of retrofit**)
	Next generation:
	Best of R_t population
	End while
	Return the best set of solutions (Pareto Front)
End	

5.1 Fragility and resilience curves

The concept of fragility curve can be used to quantify the seismic vulnerability of a system or component such as a bridge or pier. In this regard, evaluating the Probabilistic Seismic Demand Models (PSDMs) is the basis for constructing the fragility curves, which establish a relationship between EDP and IM using linear regression in logarithmic space (**Fig. 5** (a)). The fragility curves are calculated characterized by the mean structure's response of the selected seismic records by assuming a log-normal distribution function, as demonstrated in **Fig. 5**. As shown in **Fig. 5** (b - d), the fragility curves for retrofitted bridges vary according to different bridge pier retrofit designs including different arrangements, materials, and thicknesses. This difference in fragility varies based on damage states, so the fragility difference increases as the damage state changes from slight to complete. In addition, the

fragility values for retrofitted bridges are less varied than those of non-retrofitted bridges. A non-retrofitted bridge experiences much nonlinear behavior, which can be amplified by increasing the seismic intensity. Therefore, the dispersion in the results increases, especially for non-retrofitted bridges. It can be stated that seismic intensity and retrofitting designs are both critical factors to ensure the predictability of structure's response. In addition, the effect of different jacketing materials is investigated and illustrated in **Fig. 5.**

(a) Upper- and lower-bounds of PSDMs

(b) Probability of exceedance a slight damage state for steel jacketing

(c) Probability of exceedance an extensive damage state for steel jacketing

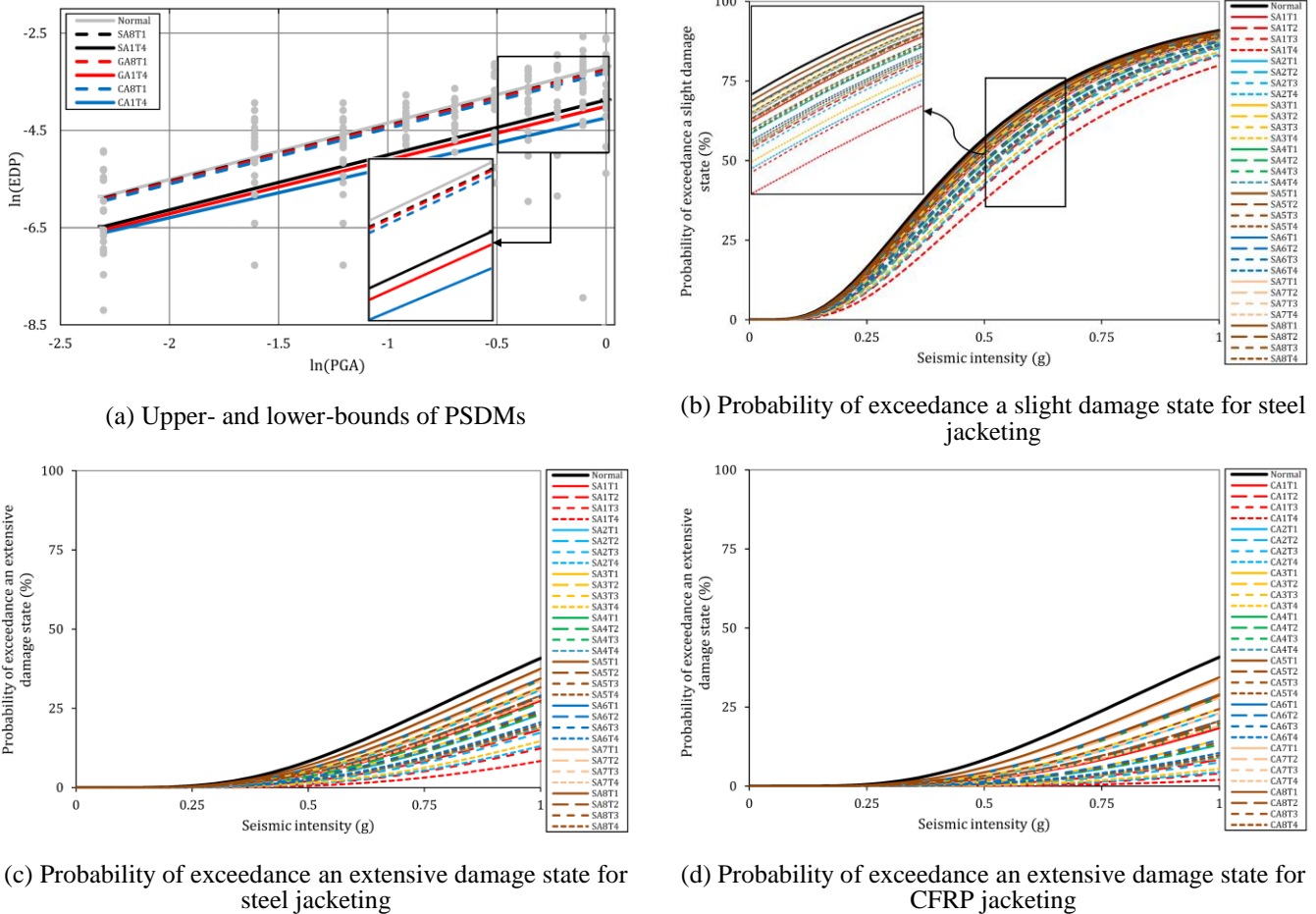(d) Probability of exceedance an extensive damage state for CFRP jacketing

Fig. 5. Fragility analysis.

The results show that CFRP jacketing has the most influence on mitigating structural damage or vulnerability following fragility curves (**Fig. 5** (c - d)). In this regard, although the thickness of SA1T2 (12.7mm) and CA1T4 (12.4mm) retrofit strategies are almost equal (see **Fig. 4**), there is a significant difference in their fragility characteristics. For instance, considering the same conditions at PGA=0.5g, the probabilities of slight damage for SA1T2 and CA1T4 are near 46.5% and 24.3%, respectively.

In the next step, resilience can be calculated based on fragility curves and recovery functions formulated and explained in Section 2. The resilience index would be considered a more understandable and sensible parameter for decision-makers rather than fragility curves, which can be used as a decision-making index as a reference for program progress in short-, mid-, and long-term planning. For this purpose, the resilience index is evaluated in the form of curves and surfaces for various retrofit designs, as shown in **Fig. 6**. The resilience curve indicates the seismic resilience value right after an earthquake with different intensities (**Fig. 6** (a - c)). As mentioned, the bridge resilience is dropped just after a seismic hazard event. It can then be restored to its intact state through repair actions. Mathematically, this drop in resilience and the effect of recovery measurement on it can be calculated using the Heaviside step (or the unit step) and restoration functions, as discussed in Section 2. In this line, the resilience surface shows how the infrastructure recovers to its intact condition due to repairs (**Fig. 6** (d)). Therefore, proper retrofit design makes the infrastructure less sensitive to destructive factors such as seismic input intensity, which leads to more predictability and reliability. In this connection, the appropriate

retrofitting strategy can provide more stable conditions for the infrastructure before, during, and post-hazardous events.
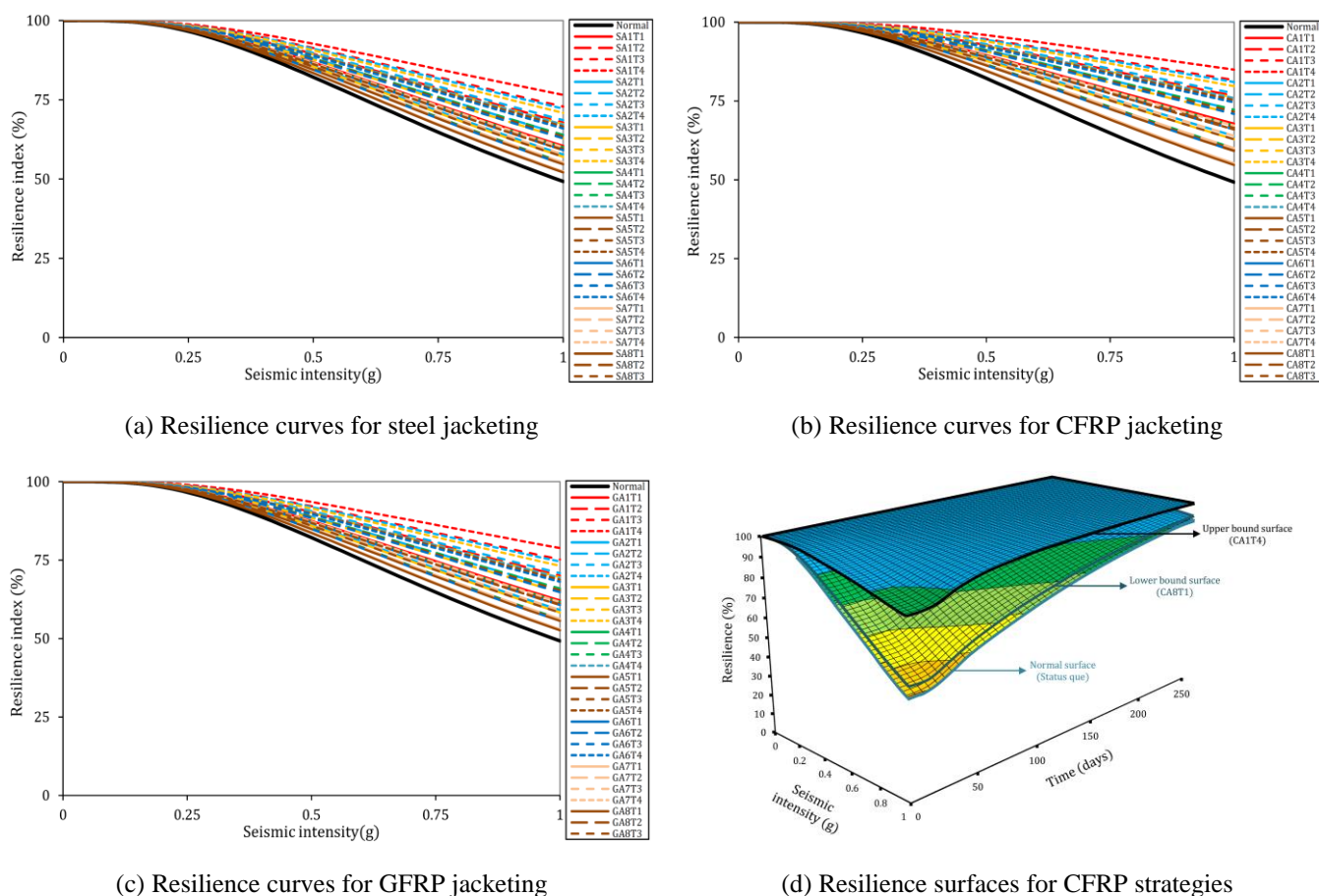

(a) Resilience curves for steel jacketing

(b) Resilience curves for CFRP jacketing

(c) Resilience curves for GFRP jacketing

(d) Resilience surfaces for CFRP strategies

Fig. 6. Resilience analysis.

5.2 Total life-cycle cost analysis

5.2.1 Total life-cycle maintenance cost

As already discussed, one of the investigated optimization objectives in this study is to minimize the LCC of existing infrastructure, including maintenance, repair, and cost of retrofit during its life-cycle. The total life-cycle maintenance cost is estimated only based on the value of the structure as formulated in Section 3, which includes the sum of the initial value (or construction cost) and the cost of retrofit (if it is retrofitted). In consideration of all applicatory cost assumptions, the total life-cycle maintenance cost for the selected retrofit design is plotted in **Fig. 7**. As evidenced by the results of **Fig. 7** (a), the increase in this cost is correlated with how much material (T1 to T4) and pier jacketing (A8 to A1) is used compared to the non-retrofitted bridge, which is the lowermost curve indicated by the black dash line. Furthermore, the effect of different times of retrofitting is examined on this cost by assuming 7-year intervals, from 0 to 70 years, as depicted in **Fig. 7** (b). The "different times of retrofitting" refers to the intervals at which retrofitting (or upgrading the existing structures) is done. For example, if a bridge is retrofitted in the 14th year, it means that the bridge will be retrofitted in 14 years after the zero time assumed in this study. This implies that the retrofitting takes place in the 14th year during the considered 75-year life-cycle.

The findings reveal that the total life-cycle maintenance cost is increased at distinct rates due to applying different retrofit strategies (**Fig. 7** (a – b)). To examine this point more comprehensively, the R/N ratio is suggested, which represents the percentage increase in the total life-cycle maintenance cost for a retrofitted bridge compared to the non-retrofitted bridge (**Fig. 7** (c)). In addition, the mean R/N ratio of different retrofit strategies is shown in **Fig. 7** (d). According to the obtained results, retrofitting

raises the total life-cycle maintenance cost by an average of about 3%.

(a) Steel jacketing

(b) SA2T2 retrofit arrangement at different times of retrofitting

(c) R/N ratio for steel jacketing

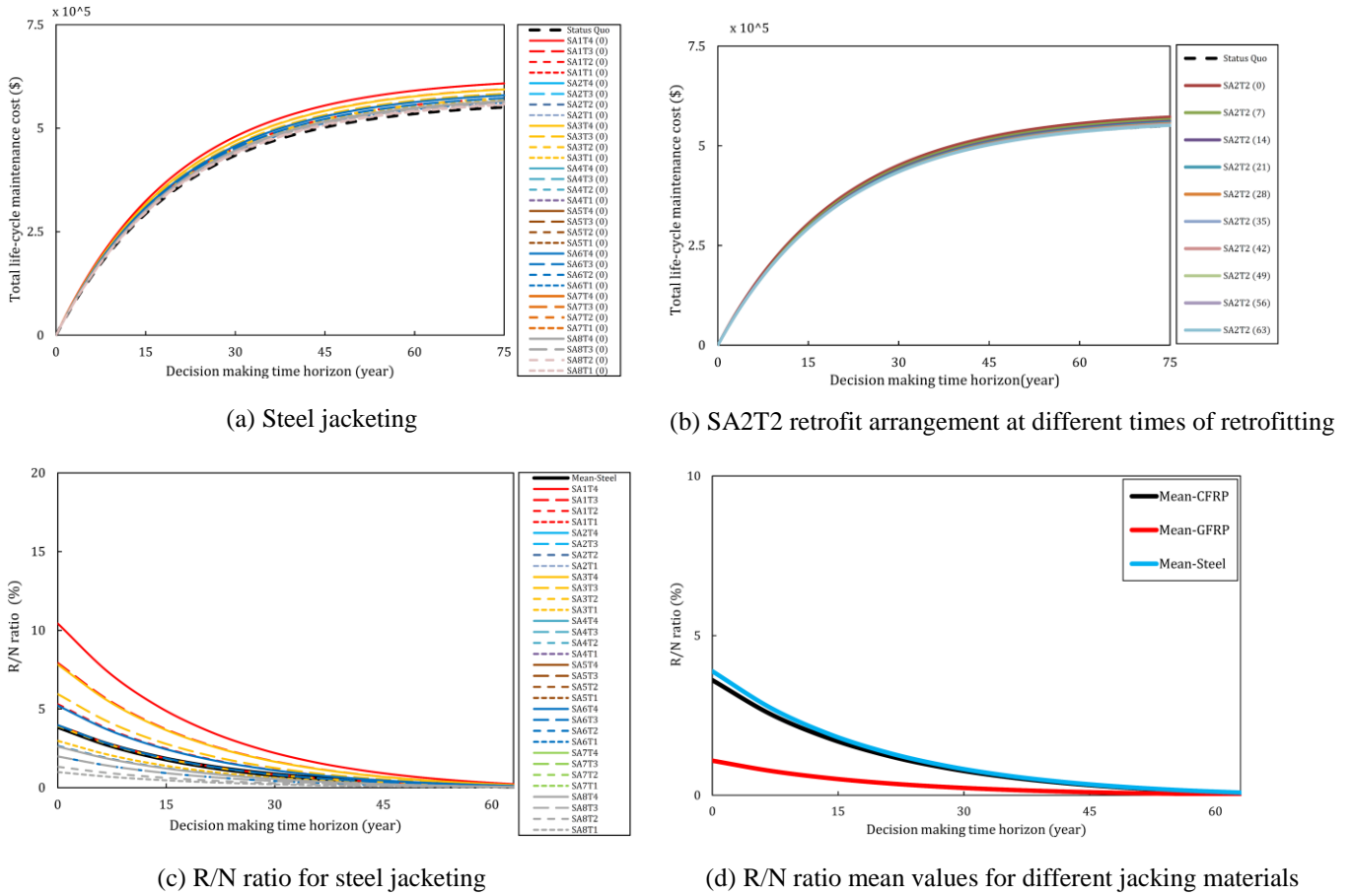(d) R/N ratio mean values for different jacking materials
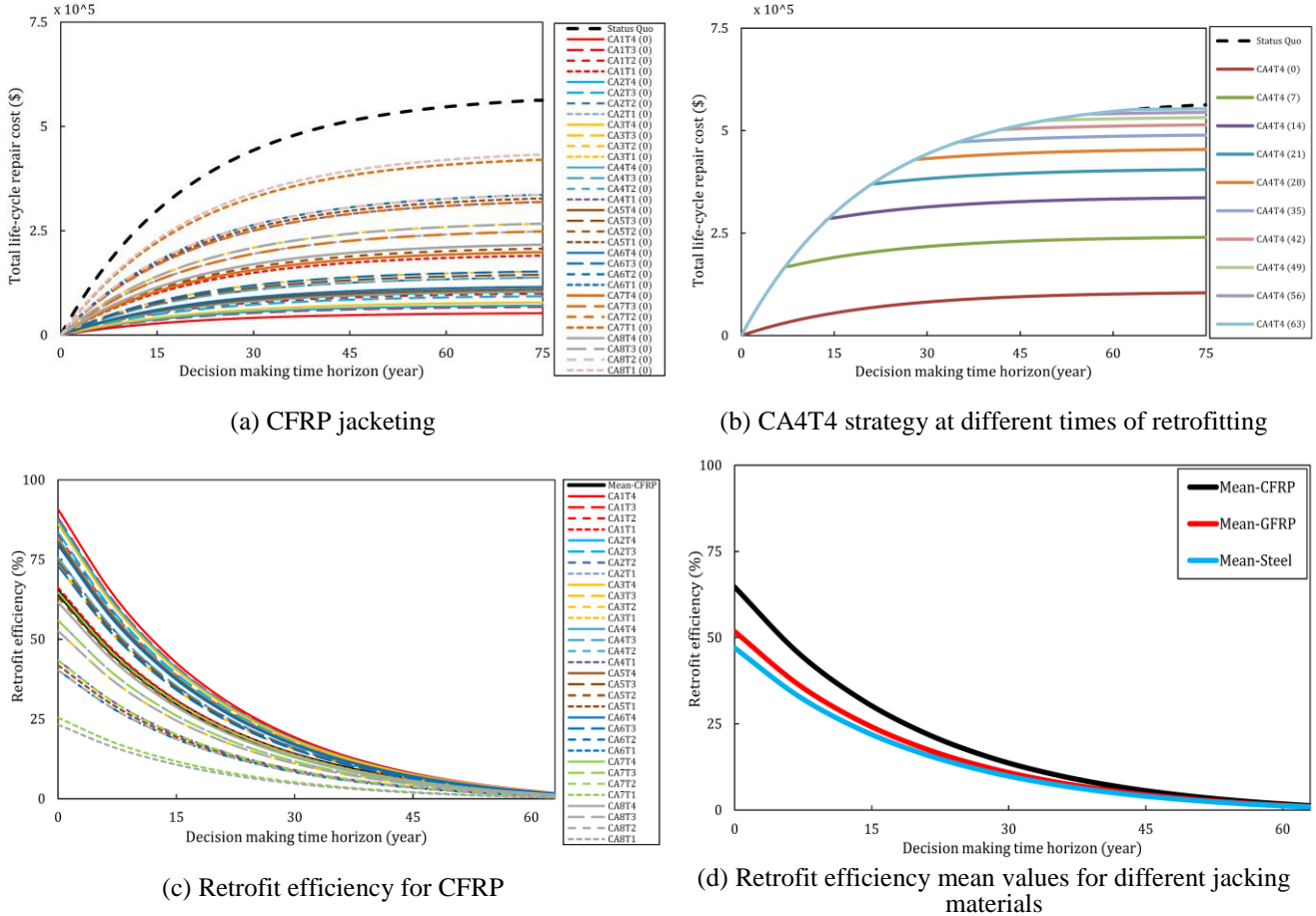
Fig. 7. The total life-cycle maintenance cost analysis.

5.2.2 Total life-cycle repair cost

The total life-cycle repair cost is the most crucial parameter in the total LCC estimation. Direct losses are included due to structural damage and indirect losses because of agency, economic, environmental, human casualties, and user losses. Also, this cost term has a decisive role in selecting the optimal retrofit strategy against seismic hazard events during its life-cycle since structural characteristic is considered in its calculation. The total life-cycle repair costs are calculated for the designated retrofit designs in light of all mentioned cost expectations (as explained in Section 4) and the presented formulation framework (refer to Section 3), as illustrated in **Fig. 8**.

As may be concluded from **Fig. 8** (a), the total life-cycle repair cost can change based on the two factors of hazard and fragility curves, which are the outputs of site hazard characteristics and dynamic structural properties, respectively. Therefore, these two factors are intrinsically involved in the computational formulation of assessing repair costs over a certain period of time, leading to the superiority of some retrofit options over others. For example, the A4 to A6 arrangements have the same number of retrofitted piers (see **Fig. 4**) and consequently are equal in the total life-cycle maintenance cost. The A4 arrangement further reduces the total life-cycle repair cost due to jacketing more central piers, which leads to a more significant reduction in the structural vulnerability against seismic input. In addition, different times of retrofitting can play a unique role in reducing/increasing this cost. The effect of this variable is plotted in **Fig. 8** (b).

As it is clear from the results of **Fig. 8** (a - b), the influence of the time of retrofitting is outstanding in decreasing the total life-cycle repair cost, so it has the maximum effect in the early years, and its impact is drastically shrunk with postponing retrofit program. This fact is justifiable and logical according to the PGA values of the hazard curve in different years and correlated fragility values. To further compare this point, the Retrofit Efficiency (RE) ratio is used, which is the ratio of "useful output"

to "total input" for the total life-cycle repair cost (**Fig. 8** (c)). In this formula, the useful output (as the numerator) is equal to the amount of reduction in the total life-cycle repair cost due to retrofitting compared to the non-retrofitted bridge, and the total input (as the denominator) is equal to the total life-cycle repair cost of the non-retrofitted bridge. As an illustration, the RE ratios of the CA1T3 (0) and CA1T3 (21) strategies are approximately 87% and 43%, respectively, which indicate the effect of the time of retrofitting along with different arrangements, thicknesses, and materials in reducing the total life-cycle repair cost compared to the non-retrofitted bridge (status quo). Also, the mean RE ratio of different retrofit strategies for the total life-cycle repair cost is represented in **Fig. 8** (d).

(a) CFRP jacketing

(b) CA4T4 strategy at different times of retrofitting

(c) Retrofit efficiency for CFRP

(d) Retrofit efficiency mean values for different jacking materials

Fig. 8. The total life-cycle repair cost analysis.

5.2.3 Life-cycle cost optimization

To fully calculate the total life-cycle cost, the total cost of retrofit must be included to the summation of the total life-cycle repair and maintenance cost terms as the Heaviside (or unit) step function during the chosen year for retrofitting. In this respect, the LCC is calculated for each retrofit design and shown in **Fig. 9**. The results indicate that implementing any retrofit design does not necessarily mean reducing or optimizing the LCC during its life-cycle compared to the non-retrofitted situation. For example, the LCC for a retrofit design such as GA1T2 is decreased compared to the non-retrofitted bridge (as a benchmark). At the same time, GA1T4 with more jacketing material increases the LCC and becomes an uneconomical solution based on only the LCC criterion (**Fig. 9** (a)). Also, it is clear that GA1T2 can reduce LCC more effectively than GA8T1 with jacketing material. Therefore, if the LCC is the only considered criterion, the repair cost and the cost of retrofit play a more important role in selecting the best retrofit designs rather than the maintenance cost. The time of retrofitting is another crucial element, especially in large-scale projects with a budget planning calendar. In this sense, the effect of retrofitting actions in different years is delineated in **Fig. 9** (b).

As it can be seen, the time of retrofitting in combination with other retrofit design variables has an undeniable effect on decreasing or increasing the LCC (**Fig. 9** (a – b)). In general, it has the maximum

impact in the early years, and its effect is drastically shrunk with the postponement of the retrofit program. Generally, if a retrofit design is planned to be applied in the early years (as a retrofit strategy), the LCC is usually reduced. On the contrary, if a retrofit strategy is implemented in later years, its effectiveness in reducing LCC is decreased, and the LCC may even increase compared to the benchmark state. Similar to the previous argument, the RE ratio is used for the LCC to carefully analyze this section's results, where positive and negative RE ratios indicate a decrease and increase in the LCC, respectively (**Fig. 9** (c - d)).
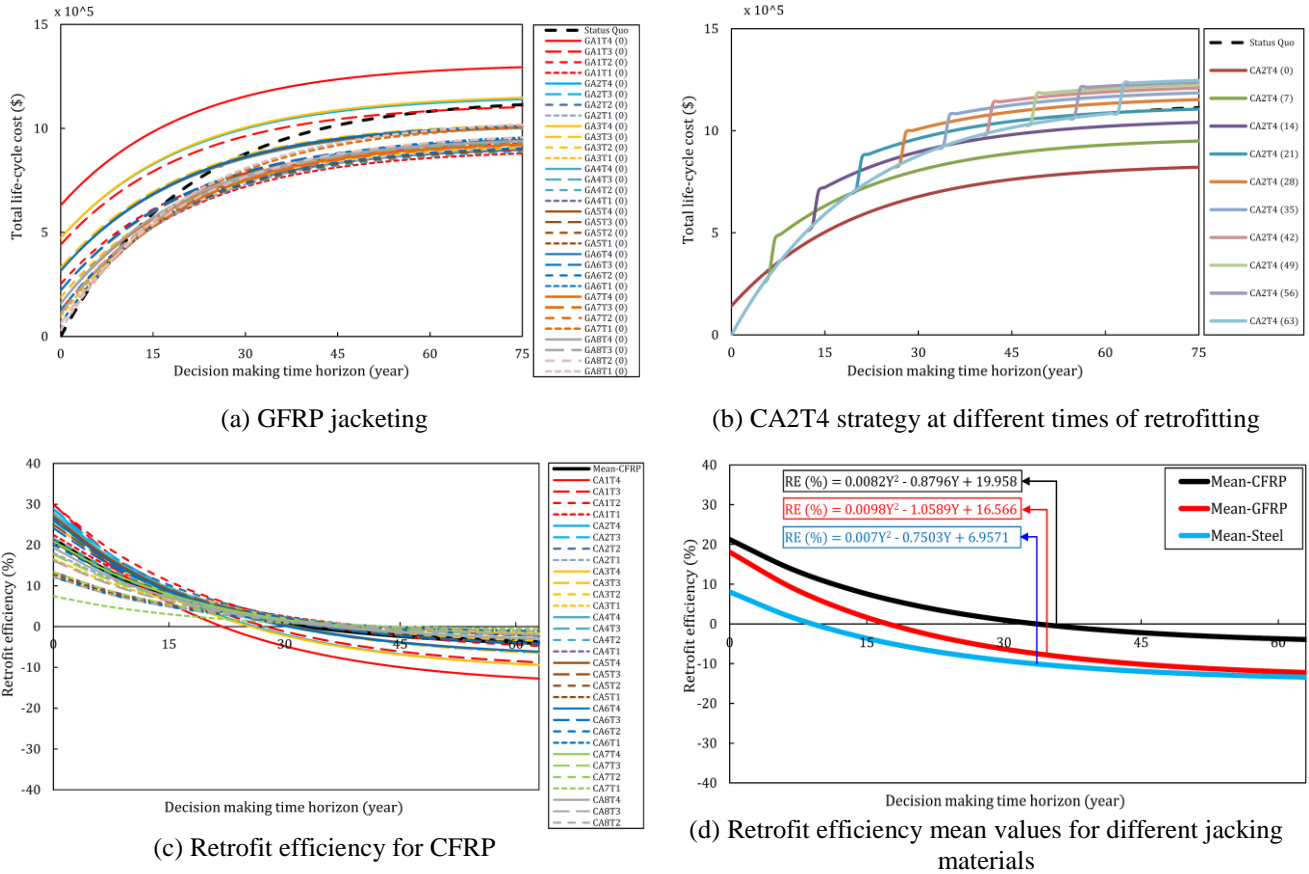

(a) GFRP jacketing

(b) CA2T4 strategy at different times of retrofitting

(c) Retrofit efficiency for CFRP

(d) Retrofit efficiency mean values for different jacking materials

Fig. 9. The life-cycle cost analysis.

Table 6. The best retrofit strategies only in regard to the life-cycle cost objective.

Rank	Strategy name	LCC ($)	RE (%)
1	GA1T2 (0)	795534.8	28.55
2	GA1T3 (0)	806494.2	27.57
3	GA2T3 (0)	811802.6	27.09
4	CA2T2 (0)	812921.4	26.99
5	CA1T2 (0)	815736.1	26.74
6	GA2T4 (0)	821738.8	26.20
7	CA1T1 (0)	823937.9	26.00
8	GA4T4 (0)	823997.7	25.99
9	GA3T3 (0)	827292.2	25.70
10	CA3T2 (0)	827358.6	25.69

The findings demonstrate that to achieve the best retrofit strategies, a balance should be struck between the cost of retrofit and the reduction of total life-cycle repair cost due to retrofitting. In this regard, retrofitting in the early years is another critical parameter in the LCC optimization framework, as given in **Table 6**. As evident, there is no steel jacketing option among the top optimal retrofit strategies because it is more expensive and less effective in reducing the total life-cycle repair cost compared to GFRP and CFRP materials. In addition, the best retrofit strategies generally include jacketing all piers with medium thickness (such as GA1T2 (0) and GA1T3 (0)) or jacketing central piers

with more thickness (such as GA4T4 (0) and GA2T4 (0)). A bridge is precious as infrastructure because of its high initial value (construction value or replacement cost) and direct and indirect losses. As a result, three major parameters in selecting the optimal retrofit strategies include (1) the importance of reducing the total life-cycle repair cost due to retrofitting, (2) the cost of retrofit, and (3) the total life-cycle maintenance cost.

5.3 Multi-objective optimization

Although the introduced LCC optimization is an acceptable and satisfactory single-objective optimization framework, there needs to be a perceptible criterion, such as resilience, to clearly express the infrastructure functionality level. In civil infrastructure management and maintenance, financial and economic issues play a dominant role in choosing the right approach to find the best retrofit strategies. As a further critical matter, the seismic resilience is critical to describe the decision-maker's performance level in the vital infrastructure sector. For this reason, two multi-objective optimization frameworks (i.e., resilience-LCC and resilience-cost of retrofit) are presented and then determined for all under-study retrofit strategies in a single-objective optimization framework (i.e., LCC). The suitability of each optimal set of solutions for different retrofit strategies is evaluated according to mentioned multi-criteria optimization, including (1) minimizing the cost of retrofit and maximizing the resilience index (as depicted in **Fig. 10**a) and (2) minimizing the LCC and maximizing the resilience index (as depicted in **Fig. 10**b). In this regard, the most optimal retrofit strategies are presented in **Table 7**.

(a) The resilience versus the cost of retrofit   (b) The resilience versus the LCC
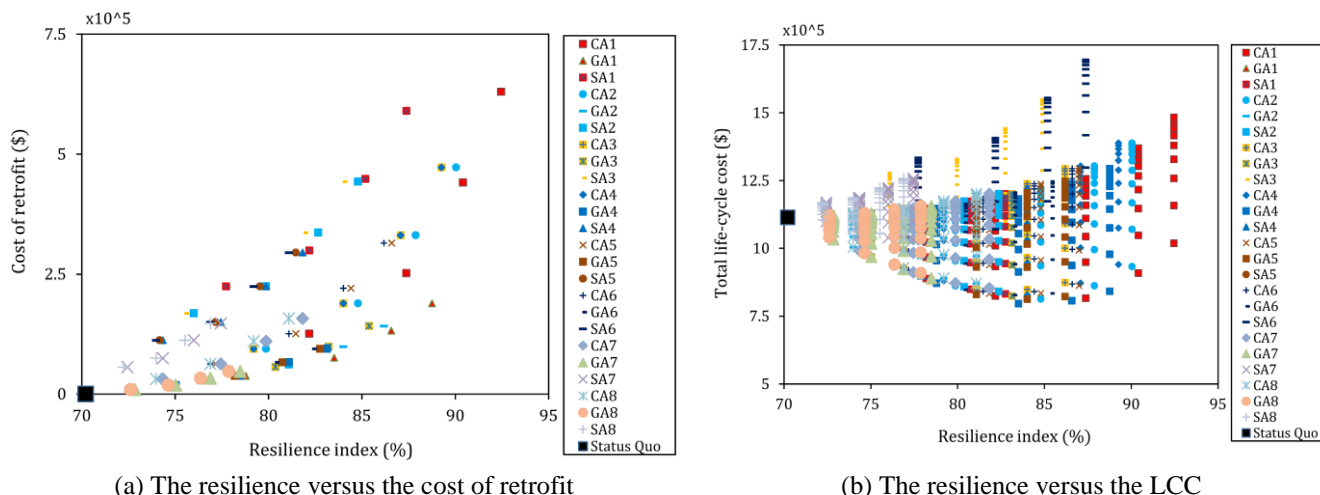
Fig. 10. Progression of optimal search for different retrofit strategies.

Table 7. The best retrofit strategies in regard to the life-cycle cost-resilience index objectives and cost of retrofit-resilience index objectives.

No.	Cost of Retrofit-R				LCC-R		
	Strategy name	Cost ($)	Resilience (%)	Resilience to cost ratio (%)	Strategy name	LCC ($)	Resilience (%)
1	GA7T1	9450	72.8	0.770828	GA1T2 (0)	795534.8	83.5
2	GA4T1	18900	75.0	0.397016	GA1T3 (0)	806494.2	86.6
3	GA2T1	28350	76.9	0.271225	CA1T2 (0)	815736.1	87.4
4	GA1T1	37800	78.8	0.208448	GA1T4 (0)	841244.7	88.8
5	GA2T2	56700	81.1	0.143013	CA1T3 (0)	908594.5	90.4
6	GA1T2	75600	83.5	0.110467	CA1T4 (0)	1017805	92.5
7	GA1T3	132300	86.6	0.065438			
8	CA1T2	252000	87.4	0.034674			
9	CA1T3	441000	90.4	0.020504			
10	CA1T4	630000	92.47	0.014677			

The output results of multi-objective optimizations can be categorized into two separate parts based on the desired objective functions. In the 1st category based on resilience-cost of retrofit

objectives, the set of the best retrofit design is divided into two segments: (I) those that have a relatively linear relationship between these two objectives, which mainly include jacketing central piers with low- to mid-thickness of cheaper but more strength materials such as GFRP compared to steel (**Fig. 11** (a)), and (II) those that do not have a linear relationship between these two objectives, which include jacketing most or all of the bridge piers with mid- to high- thickness of materials with more effectiveness in reducing vulnerability such as CFRP (**Fig. 11** (b)). In the 2nd category based on resilience-LCC objectives, the most optimal retrofit strategies include jacketing all of the bridge piers with mid- to high- thickness of CFEP and GFRP in the first years of retrofitting program, because the functionality and cost-benefit effects are simultaneously and directly considered in this framework. In this regard, the rationality of using the proposed LCC-resilience optimization is emphasized by comparing the obtained results from SOO, MOO-1, and MOO-2 frameworks.
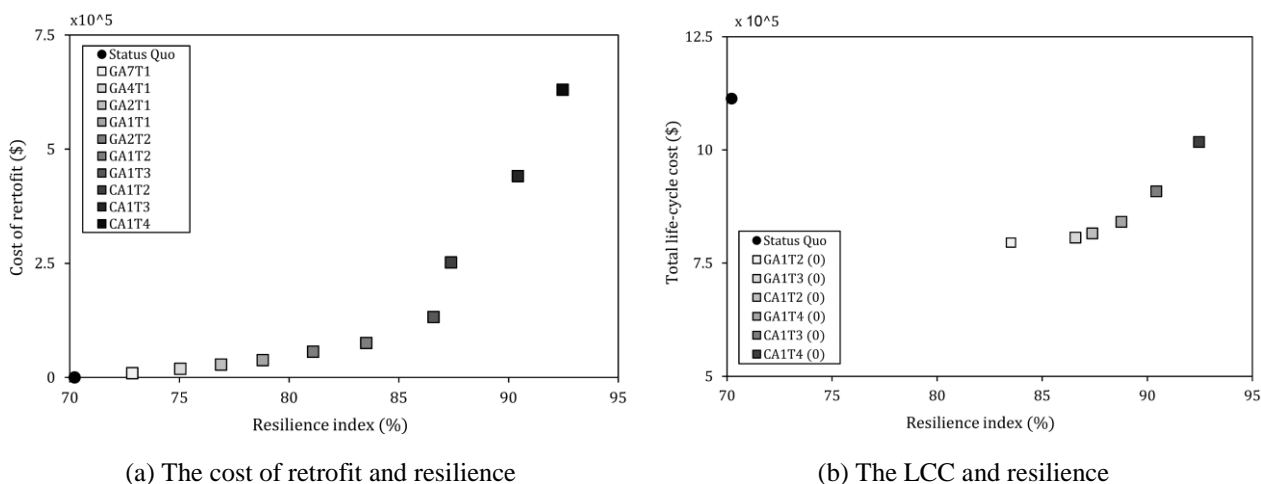

(a) The cost of retrofit and resilience   (b) The LCC and resilience

Fig. 11. General trend of the most optimal solutions.

6 Conclusions

This study proposes a sense-making optimization framework in infrastructure management for decision-making to prepare the most optimal retrofit strategies. For this purpose, a typical bridge is considered a case study because of its critical functions in the transportation network. In this regard, different optimization frameworks with various objectives are investigated and compared in the form of single- and multi-objective optimizations. Consequently, the most optimal retrofit strategies are presented and discussed for the studied optimization approaches (i.e., LCC, R-cost of retrofit, and R-LCC) by considering multiple retrofit strategies, including different materials, thicknesses, arrangements, and timing of retrofitting actions. Specific conclusions of this research based on the obtained results are summarized as follows:

(1) The fragility curves are uniquely constructed based on structural and site characteristics, including retrofit designs and seismic input loads, respectively. The difference between the computed fragility value, particularly for non-retrofitted bridge, is increased with the increase of the seismic intensity and the severity of the damage state from slight to complete.

(2) The resilience curves/surfaces indicate that selecting a suitable retrofit design for the studied infrastructure leads to better predictability and reliability against uncertainties and, thus, less sensitivity to destructive factors. Also, the importance of retrofitting the central piers is evidenced in this index.

(3) The total life-cycle maintenance cost is only correlated with the sum of the initial value (or construction cost) and the cost of retrofit. According to the R/N ratio, this cost increases by about 3% due to retrofit actions.

(4) The total life-cycle repair cost is changed based on site hazard characteristics, dynamic structural properties, and direct and indirect losses. Additionally, the time of retrofitting (as a key parameter in retrofit strategy) remarkably reduces repair costs. The positive influence of applying retrofitting actions in the early years is evident by introducing the RE ratio, and this effect is decreased by postponing the retrofit program.

(5) The total life-cycle cost output results demonstrate that each retrofit strategy has a different effect on reducing or increasing the LCC compared to the non-retrofitted bridge. In this respect, retrofitting actions in the first years have maximum impact. However, it is drastically reduced by postponing it in a way that may even increase the LCC. In addition, to achieve the best retrofit strategy based on the LCC criterion, a balance should be struck between the two key parameters of reducing the total life-cycle repair cost due to retrofitting and the cost of retrofit.

In this study, a multi-objective optimization framework is proposed to find the most optimal retrofit strategies that maximize the resilience index while minimizing the LCC. By comparing different optimization frameworks (i.e., SOO, MOO-1, and MOO-2), it can be concluded that the proposed LCC-resilience eliminates less appropriate strategies because the level of functionality and cost-benefit are simultaneously directly considered in this approach.

Finally, it should be noted that aging and multi-component vulnerability are other significant parameters for the seismic resilience assessment of bridges. In future works, these effects should also be considered in seismic resilience and life-cycle cost studies.

Funding Statement

CRediT authorship contribution statement

Pedram Omidian: Conceptualization, Investigation, Formal analysis, Writing – original draft. **Naser Khaji**: Conceptualization, Supervision, Writing – review & editing. **Ali Akbar Aghakouchak**: Conceptualization, Supervision, Writing – review & editing.

Conflicts of interest

The authors declare no conflict of interest.

Acknowledgments

References

[1] Quintero MAM, Tam CPT, Li H. Structural analysis of a Guadua bamboo bridge in Colombia. Sustainable Structures 2022; 2(2): 000020. https://doi.org/10.54113/j.sust.2022.000020

[2] Fereshtehnejad H, Shafieezadeh A. A multi-type multi-occurrence hazard lifecycle cost analysis framework for infrastructure management decision making. Engineering Structures 2018; 167: 504–517. https://doi.org/10.1016/j.engstruct.2018.04.049

[3] Omidian P, Khaji N. A total life-cycle cost–resilience optimization framework for infrastructures management using different retrofit strategies. Sustainable and Resilient Infrastructure 2023; 1-24. https://doi.org/10.1080/23789689.2023.2257516

[4] Iryo T, Iiyama K, Lalith M, Hori M. On computational costs for Monte Carlo regional-scale simulation for reliable estimate of city and urban area earthquake disaster. Journal of Earthquake and Tsunami 2022; 16(3): 224003. https://doi.org/10.1142/S1793431122400036

[5] Zhu Y, Zhao Sh, Zhang Y. Deformation and energy dissipation of steel box girders of cable-stayed bridges subjected to blast loadings. Sustainable Structures 2023; 3(2): 000032. https://doi.org/10.54113/j.sust.2023.000032

[6] Zhang D, Gong M, Zhang S, Zhu X. A review of tiny houses in North America: Market demand. Sustainable Structures 2022; 2(1): 000012. https://doi.org/10.54113/j.sust.2022.000012

[7] Liang Y, Kong Y-Z, Zhao C-X, Liu R-Q, Luo J, Zhu R-H. Time-varying seismic fragility analysis of ECC-RC composite bridge with high-strength steel bars. Journal of Earthquake and Tsunami 2024; 18(1), Article 2350029. https://doi.org/10.1142/S179343112350029X

[8] Takahashi Y, Der Kiureghian A, Ang AH-S. Life-cycle cost analysis based on a renewal model of earthquake occurrences. Earthquake Engineering and Structural Dynamics 2004; 33: 859–880. https://doi.org/10.1002/eqe.383

[9] Frangopol DM, Liu M. Maintenance and management of civil infrastructure based on condition, saf

ety, optimization, and life-cycle cost. Structure and Infrastructure Engineering 2007; 3(1): 29–41. https://doi.org/10.1080/15732470500253164

[10] Kia M, Amini A, Bayat M, Ziehl P. Probabilistic seismic demand analysis of structures using reliability approaches. Journal of Earthquake and Tsunami 2021; 15(3): Article 2150011. https://doi.org/10.1142/S1793431121500111

[11] Zhu J, Liu B. Performance life cost-based maintenance strategy optimization for reinforced concrete girder bridges. Journal of Bridge Engineering 2013; 18(2): 172–178. https://doi.org/10.1061/(ASCE)BE.1943-5592.0000344

[12] Omidian P, Khaji N. A multi-objective optimization framework for seismic resilience enhancement of typical existing RC buildings. Journal of Building Engineering 2022; 52, Article 104361. https://doi.org/10.1016/j.jobe.2022.104361

[13] Timsina K, Amatya N, Gadagamma CK, Meguro K. Retrofitting solution for soft story mitigation in reinforced concrete frame buildings: a socio-technical approach using numerical optimization. Journal of Earthquake and Tsunami 2024 (Online Ready) https://doi.org/10.1142/S1793431123500409

[14] Fu Zh, Wu D, Fang L, Chen D, Ji B. Design, optimization and nonlinear response control analysis of the Mega Sub-Controlled Structural System (MSCSS) under earthquake action. Journal of Earthquake and Tsunami 2022; 14(3): Article 2050013. https://doi.org/10.1142/S179343112050013X

[15] Deb K, Prata A, Agarwal A, Meyarivan T. A fast and elitist multi-objective genetic algorithm: NSGA-II. IEEE Transactions on Evolutionary Computation 2002; 6(2): 182–197. https://doi.org/10.1109/4235.996017

[16] Capozzo M, Rizzi A, Cimellaro GP, Domaneschi M, Barbosa A, Cox D. Multi-hazard resilience assessment of a coastal community due to offshore earthquakes. Journal of Earthquake and Tsunami 2019; 13(2): Article 1950008. https://doi.org/10.1142/S1793431119500088

[17] Bruneau M, Reinhorn AM. Exploring the concept of seismic resilience for acute care facilities. Earthquake Spectra 2007; 23: 41–62. https://doi.org/10.1193/1.2431396

[18] HAZUS–MH MR5. Multi-hazard loss estimation methodology–earthquake model, Department of Homeland Security, Washington DC, 2014. Accessed URL:<https://www.hsdl.org/c/view?docid=12760>

[19] Uenaga T, Omidian P, George RC, Mirzajani M, Khaji N. Seismic resilience assessment of curved reinforced concrete bridge piers through seismic fragility curves considering short- and long-period earthquakes. Sustainability 2023; 15(10): 7764. https://doi.org/10.3390/su15107764

[20] Raghunandan M, Liel AB, Luco N. Aftershock collapse vulnerability assessment of reinforced concrete frame structures. Earthquake Engineering & Structural Dynamics 2015; 44(3): 419–439. https://doi.org/10.1002/eqe.2478

[21] Sultan M, Kawashima K. Comparison of the seismic design of highway bridges in California and in Japan, Recent selected publications of Earthquake Engineering Div., Public Works Research Institute (PWRI), Japan (Technical Memorandum of PWRI No. 3276), 1993. Accessed URL:< https://thesis.pwri.go.jp/public_detail/109658/>

[22] SeismoStruct. SeismoSoft, A computer program for static and dynamic nonlinear analysis of framed structures, 2023. Accessed URL:<https://seismosoft.com/product/seismostruct/>

[23] Madas P, Elnashai AS. A new passive confinement model for the analysis of concrete structures subjected to cyclic and transient dynamic loading. Earthquake Engineering & Structural Dynamics 1992; 21: 409–431. https://doi.org/10.1002/eqe.4290210503

[24] Martinez-Rueda JE, Elnashai AS. Confined concrete model under cyclic load. Materials and Structures 1997; 30: 139–147. https://doi.org/10.1007/BF02486385

[25] Yassin MHN. Nonlinear analysis of prestressed concrete structures under monotonic and cyclic loads, Ph.D. Thesis, University of California, Berkeley, USA, 1994. Accessed URL:<https://search.worldcat.org/en/title/222312210>

[26] Filippou FC, Popov EP, Bertero VV. Effects of bond deterioration on hysteretic behaviour of reinforced concrete joints, Report EERC 83-19, Earthquake Engineering Research Center, University of California, Berkeley, USA, 1983. Accessed URL:<https://nehrpsearch.nist.gov/static/files/NSF/PB84192020.pdf>

[24] Monti G, Nuti C, Santini S. CYRUS - Cyclic Response of Upgraded Sections, Report No. 96-2, University of Chieti, Italy, 1996. Accessed URL:<https://hdl.handle.net/11590/191035>

[28] Fragiadakis M, Pinho R, Antoniou S. Modelling inelastic buckling of reinforcing bars under earthquake loading, In book: Computational Structural Dynamics and Earthquake Engineering: Structures and Infrastructures Book Series, Vol. 2 (1st ed.), CRC Press, 2008. https://doi.org/10.1201/9780203881637

[29] Ferracuti B, Savoia M. Cyclic behavior of CFRP-wrapped piers under axial and flexural loading. In Proceedings of the International Conference on Fracture, Turin, Italy, 2005. Accessed URL:<https://citeseerx.ist.psu.edu/document?repid=rep1&type=pdf&doi=8b61f15de5c256d85fbf9eb8e8e02d4d1872aa3

3>

[30] Yankelevsky DZ, Reinhardt HW. Uniaxial behavior of concrete in cyclic tension. Journal of Structural Engineering 1989; 115: 166–182. https://doi.org/10.1061/(ASCE)0733-9445(1989)115:1(166)

[31] Spoelstra MR, Monti G. FRP-confined concrete model. Journal of Composites for Construction 1999; 3: 143–150. https://doi.org/10.1061/(ASCE)1090-0268(1999)3:3(143)

[32] FIB (Fédération International du Béton). Retrofitting of concrete structures by externally bonded FRPS, with emphasis on seismic applications, FIB Bulletin No. 35, Federation Internationale du Beton, 220, 2006. https://doi.org/10.35789/fib.BULL.0035

[33] Shome N, Cornel CA. Probabilistic seismic demand analysis of nonlinear structures, Reliability of Marine Structures Program Technical Report RMS-35, Stanford Digital Repository, 1999. Accessed URL:<https://purl.stanford.edu/qp089qb1141>

[34] PEER. Pacific Earthquake Engineering Research Center, online strong motion database, 2023. Accessed URL:<https://ngawest2.berkeley.edu/>

[35] Caltrans. Historic bridge inventory, sample plans of actions. Division of Maintenance, Structure Maintenance, 2005. Accessed URL:<http://www.dot.ca.gov/hq/structur/strmaint/poa_samp.pdf>

[36] Fereshtehnejad E, Hur J, Shafieezadeh A, Brokaw M. Ohio bridge condition index: multilevel cost-based performance index for bridge systems. Transportation Research Record: Journal of the Transportation Research Board 2017; 2612: 152–160. https://doi.org/10.3141/2612-17

[37] Copeland LuAnn. User's manual for QYEWZ-98. College Station, Texas: Texas Transportation Institute, The Texas A&M University System, 1988. Accessed URL:<https://tti.tamu.edu/>

[38] Caltrans. Annual average daily truck traffic on the California state highway system, Traffic Data Branch, 2016. Accessed URL:<https://dot.ca.gov/-/media/dot-media/programs/traffic-operations/documents/census/f0017681-2016-aadt-truck-a11y.pdf>

[39] Bocchini P, Frangopol DM. Optimal resilience-and cost-based postdisaster intervention prioritization for bridges along a highway segment. Journal of Bridge Engineering 2010; 17(1): 117–29. https://doi.org/10.1061/(ASCE)BE.1943-5592.0000201

[40] The Ohio Department of Transportation, Innovative Contracting Manual, Division of Construction Management, 2010. Accessed URL:<https://www.dot.state.oh.us/Divisions/ConstructionMgt/Admin/Innovative%20Contracting/Innovative_Contracting_Manual.PDF>

[41] Kliesen KL, Mill JS. The economics of natural disasters. The regional economist. Federal Reserve Bank of St. Louis, p. 332, 1994. Accessed URL:<https://www.stlouisfed.org/publications/regional-economist/april-1994/the-economics-of-natural-disasters>

[42] Soliman M, Frangopol DM. Life-cycle cost evaluation of conventional and corrosion resistant steel for bridges. Journal of Bridge Engineering 2014; 20(1): Article 06014005. https://doi.org/10.1061/(ASCE)BE.1943-5592.0000647

[43] Gallivan F, Ang-Olson J, Papson A, Venner M. Greenhouse gas mitigation measures for transportation construction, maintenance, and operations activities. San Francisco: AASHTO Standing Committee on the Environment, 2010. Accessed URL:<http://onlinepubs.trb.org/onlinepubs/nchrp/docs/NCHRP25-25(58)_FR.pdf>

[44] Kendall A, Keoleian GA, Helfand GE. Integrated life-cycle assessment and life-cycle cost analysis model for concrete bridge deck applications. Journal of Infrastructure Systems 2008; 14(3): 214–22. https://doi.org/10.1061/(ASCE)1076-0342(2008)14:3(214)

[45] Porter K, Shoaf K, Seligson H. Value of injuries in the Northridge earthquake. Earthquake Spectra 2006; 22(2): 555–563. https://doi.org/10.1193/1.2194529

[46] Caltrans. High occupancy vehicle lanes status report. Sacramento metropolitan area. District 3. Office of Freeway Operations, Sacramento, 2011. Accessed URL:<https://dot.ca.gov/programs/traffic-operations/hov>

[47] Afshari H, Hare W, Tesfamariam S. Constrained multi-objective optimization algorithms: review and comparison with application in reinforced concrete structures. Applied Soft Computing 2019; 83: Article 105631. https://doi.org/10.1016/j.asoc.2019.105631

[48] Rahimi I, Gandomi AH, Nikoo MR, Chen F. A comparative study on evolutionary multi-objective algorithms for next release problem. Applied Soft Computing 2023; 144: Article 110472. https://doi.org/10.1016/j.asoc.2023.110472

[49] Ghodousian O, Behdad K, Shafaie V, Ghodousian A, Mehdikhani H. Predicting 28-day compressive strength of pozzolanic concrete by generalized nearest neighborhood clustering using modified PSO algorithm. Malaysian Construction Research Journal 2021; 33(1), 61-72. Accessed URL:<https://www.cream.my/prod/mcrj-volume-33-no-1-2021>